Wind-induced response of an offshore wind turbine under non-neutral conditions: A comparison with Hywind Scotland

Wind-induced response of an offshore wind turbine under non-neutral conditions: A comparison with Hywind Scotland

Rieska Mawarni Putri and Charlotte Obhrai

Department of Mechanical and Structural Engineering and Materials Science, University of Stavanger, Norway

E-mail: rieska.m.putri@uis.no

Abstract. In this study, aeroelastic simulations of a 5 MW spar wind turbine are performed by using simulated wind fields that are representative of surface layer marine atmospheric turbulence under different atmospheric stratifications. The spar floater's motion responses from the simulations are then compared with the observations from Hywind Scotland's 6 MW spar wind turbine. The platform's pitch and yaw motions from the simulations are consistent with the observations, in terms of mean wind speed and atmospheric stratification. The simulations and the observations show that a stable atmosphere induces the lowest platform pitch and yaw motions compared to neutral and unstable stratifications. Nonetheless, the discrepancy of platform motions between stable and unstable conditions is more pronounced from the observations than in the simulations. Uncertainties associated with the estimation of the atmospheric stability and the modelling of the turbulence's co-coherence for lateral separation may partly account for the discrepancies between the observed and the simulated motion responses of the spar wind turbine.

1. Introduction

In 2020, Jacobsen and Godvik [1] documented the spar floater motions from the first commercial floating wind farm, the Hywind Scotland, as a function of atmospheric stability. Hywind Scotland Wind Farm consists of five 6 MW spar wind turbines, which are located approximately 25 km from the coast of Peterhead, Scotland [1]. Due to its location, the wind farm is located in the marine atmospheric boundary layer (MABL), which is known for its variable atmospheric stability conditions throughout a year [2]. The study by Jacobsen and Godvik [1] clearly shows that atmospheric stability affects the spar wind turbines' floater motion responses in both free wind and wake conditions. The most significant effect was observed for the platform yaw motion of the spar floater under a stable atmosphere.

The influence of surface layer atmospheric stability on offshore wind turbine (OWT) load responses has been previously studied by e.g. Sathe et al. [3] and Holtslag et al. [4]. In Sathe et al. [3], the wind-induced response of a bottom-fixed wind turbine was found to depend on the atmospheric stability. In their study, the uniform shear turbulence model (Mann model) [5] which is outlined in the IEC 61400-1 [6], was used. Additionally, site-specific measurements were fitted to the uniform shear model for different atmospheric stability conditions. However, the uniform shear model was originally intended to be used only for neutral surface layer atmospheric stratification. Therefore, it cannot fully capture the effects of buoyancy-generated turbulence in non-neutral stratifications ([5, 7]).

There exist only a few turbulence models developed specifically for non-neutral atmospheric stability conditions, including the modified spectral tensor model [7], the Højstrup spectral model [8], and the Pointed-Blunt model [9]. The modified spectral tensor model was shown to work reasonably well for surface layer stable atmosphere, but not for unstable conditions, especially at low wave frequencies [7]. Whereas, the Højstrup spectral model was developed only for unstable stratification and its effect on floating wind turbine (FWT) load and motion responses has been studied previously by Putri et al. [10]. The Pointed-Blunt model was established based on measurements from an offshore observation platform, FINO1, at fixed elevations of 40, 60, and 80 m for various atmospheric stratifications [9]. The Pointed-Blunt model is representative of MABL, but it is limited in terms of height, particularly for heights higher than 80 m.

Using the Pointed-Blunt model, the present paper simulates the floater motion responses of a spar wind turbine exposed to wind flows under varying atmospheric stratifications (i.e. stable, neutral, and unstable). The simulated responses are compared to the observed responses from Hywind Scotland to determine if the Pointed-Blunt spectral model is able to represent the non-neutral conditions in the MABL.

2. Methodology

The wind fields for different surface layer atmospheric stratifications used in this study were generated following Cheynet [11] for the Pointed-Blunt model. Then, aero-hydro-servo-elastic simulations were performed on the 5 MW OC3 spar wind turbine [12] using these wind fields. Although an OWT may be partly located above the surface layer, the Pointed-Blunt model was used herein for simplicity.

2.1. Observations from Hywind Scotland

Hywind Scotland Wind Farm comprises five wind turbines (WTs) arranged in two rows with a distance of nine rotor diameters between neighbouring WTs [1]. Only observations from the WT exposed to free wind flow are discussed in the present study to focus on the influence of atmospheric stability on the spar WT responses.

Some key properties of the Hywind Scotland's WT are given in Table 3. In Jacobsen and Godvik [1], the observed floater motions (roll, pitch, and yaw) were studied using 10 min time series from December 2017 to July 2018. Their dataset excluded observations when the wind speed at the hub height was less than $3\,\mathrm{m\,s^{-1}}$, when there was limited power production, and when the nacelle yaw was larger than 5°. Due to the limited instrumentation at the Hywind Scotland site, the atmospheric stability was determined by measuring the temperature difference between the air and the sea ($\Delta T = T_{air} - T_{sea}$) [1]. The atmosphere's stability was flagged as unstable when $\Delta T < -1.5°C$, neutral if $-1.5°C < \Delta T < 0.5°C$, and stable for $\Delta T > 0.5°C$.

2.2. Step 1: Wind field generation

The thermal stratification of the atmosphere is quantified by the non-dimensional stability parameter $\zeta = z/L$, where z is a reference height [m] and L is the Obukhov length [m], in the present study. L is proportional to the ratio between the cube of the friction velocity (u_*^3) and the virtual potential temperature flux [13]. An unstable atmosphere occurs when the turbulence is enhanced by buoyancy, while a stable atmosphere occurs when the turbulence is inhibited by buoyancy. In the present study, five stability classes are considered, ranging from $\zeta = -0.5$ to $\zeta = 0.5$ as given in Table 1. Wind field generation was performed using MATLAB [11], which requires three inputs: the mean wind speed, the one-point spectrum, and the co-coherence of turbulence, which is the real part of the root-coherence [14]. The wind time series were generated using the spectral representation method ([15, 16]). For each stability class, eight mean wind speeds ($\overline{u}_{hub}$) were considered (Table 2), so there are 40 cases in total. Each case was generated as a 30 min wind time series with a sampling rate of 9.1 Hz. To help reduce uncertainty, each

Table 1. Atmospheric stability classification.

Stability	ζ
Moderately unstable	$-0.5 \leq \zeta < -0.3$
Slightly unstable	$-0.3 \leq \zeta < -0.1$
Near-neutral	$-0.1 \leq \zeta < 0.1$
Slightly stable	$0.1 \leq \zeta < 0.3$
Moderately stable	$0.3 \leq \zeta < 05$

case was simulated using six different random seeds, where the median values were chosen as the averaging method.

The empirical formula for the Pointed-Blunt spectral model, which is valid for near-neutral and unstable stratifications [9]:

$$\frac{fS_i}{u_*^2} = \frac{a_1^i n}{(1 + b_1^i n)^{5/3}} + \frac{a_2^i n}{1 + b_2^i n^{5/3}} \tag{1}$$

for a stable atmosphere, the following applies [9]:

$$\frac{fS_i}{u_*^2} \approx c_1 n^{-2/3} + \frac{a_2^i n}{1 + b_2^i n^{5/3}} + a_3 n^{-2}. \tag{2}$$

where S_i, $i = u, v, w$ is the one-point spectrum of turbulence component. Coefficients a_1^i, a_2^i, a_3, b_1^i, b_2^i, and c_1 are a function of stability and for brevity, the values are not provided here, but are available in Cheynet et al. [9]. f is the frequency [Hz], $n = fz/\overline{u}_{hub}$ is the dimensionless frequency, and u_* is the friction velocity [$\mathrm{m\,s^{-1}}$].

The friction velocity is estimated following Section 2.3.6 in DNV-RP-C205 [17]:

$$\overline{u}_{hub} = \frac{u_*}{\kappa}\left(\ln\frac{z}{z_0} - \psi\right) \tag{3}$$

where $\overline{u}_{hub}$ is the mean wind speed at a reference height, in this case at the hub elevation. $\kappa \approx 0.4$ is the von Kármán constant, z_0 is the surface roughness, and ψ is a stability function [17]:

$$\psi = \begin{cases} -4.8\zeta & \zeta \geq 0 \\ 2\ln(1+x) + \ln(1+x^2) - 2\tan^{-1}(x) & \zeta < 0 \end{cases} \tag{4}$$

where $x = (1 - 19.3\zeta)^{1/4}$. The surface roughness z_0, is computed using the Charnock relation by assuming near-neutral stability for simplicity [18]:

$$z_0 = \frac{\alpha_c u_*^2}{g} \tag{5}$$

α_c is a constant, taken as 0.0185 [19] and $g = 9.81\,\mathrm{m\,s^{-1}}$ is the acceleration of gravity. Fig. 1 summarises the estimated friction velocity for each stability class and mean wind speed. The friction velocity increases almost linearly with the mean wind speed and as ζ decreases, as expected.

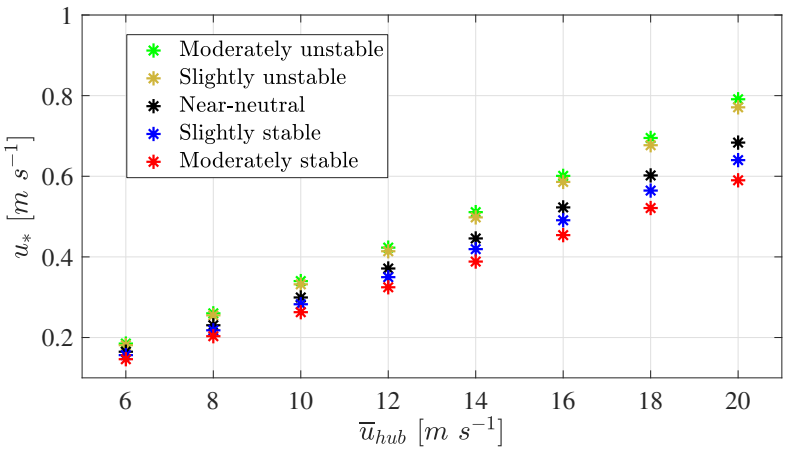

Figure 1. Estimated friction velocity for the considered atmospheric stability classes, as a function of mean wind speed at hub height.

The stability-dependant co-coherence was taken from the empirical formula [9], which was developed based on the Davenport coherence function [20]. The formulation is applicable only for vertical separations. In the absence of information on the lateral-separation co-coherence, it was then assumed that the lateral-separation co-coherence has the same magnitude as the vertical-separation co-coherence, that is

$$\gamma_i(d,f) \approx \exp\left\{-\left[\frac{d}{\overline{u}_{hub}}\sqrt{(c_1^i f)^2+(c_1^i)^2}\right]\right\} \tag{6}$$

where d is the separation distance [m] either in the lateral or vertical direction, c_1^i and c_2^i are stability-dependant coefficients.

The dimensionless target spectra of the Pointed-Blunt model at near-hub height for $\overline{u}_{hub} = 12\,\mathrm{m\,s^{-1}}$ are presented in Fig. 2. The spectra are normalised with the dissipation of turbulence kinetic energy [13]:

$$\phi_\epsilon^{2/3} = \begin{cases} 1+0.5|\zeta|^{2/3}, & \zeta \le 0 \\ (1+5\zeta)^{2/3}, & \zeta \ge 0 \end{cases} \tag{7}$$

For comparison, the well-known empirical spectra for near-neutral stratification from Kansas measurement (Kaimal spectral model) [13] are shown as dashed lines. The atmospheric stability affects the turbulent component spectra, especially when $n < 0.4$. At this range, the spectral energies are higher under unstable conditions than under stable conditions, for all three velocity components.

Similarly, the stability-dependent co-coherence is plotted in Fig. 3 and was compared with the IEC exponential coherence [6]. Here, the separation distance d is taken as 60 m, which is applicable for either lateral or vertical separation, and $\overline{u}_{hub} = 12\,\mathrm{m\,s^{-1}}$. The magnitude of the co-coherences increases gradually from moderately stable to moderately unstable conditions, which is not included in the exponential coherence model [6]. The IEC exponential coherence provides significantly lower co-coherences for the cross-wind component at $kd < 0.2$ and vertical wind component for all kd, due to (1) the lower magnitudes of turbulence length scale for the v-component (113 m) and w-component (28 m) than the u-component (340 m) and (2) a constant decay coefficient of 12 for all three velocity components.

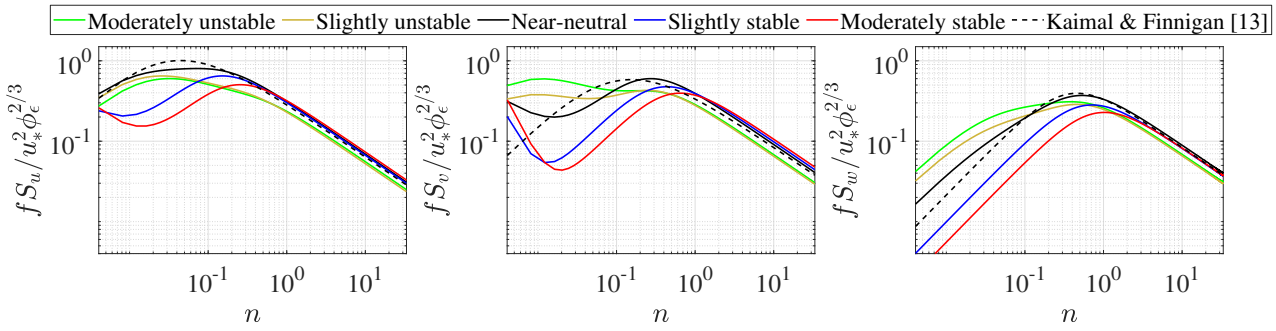

Figure 2. Empirical spectra of the along-wind (left), cross-wind (middle), and vertical (right) velocity components for all considered stability classes for $\overline{u}_{hub} = 12\,\mathrm{m\,s^{-1}}$. The velocity spectrum from Kaimal and Finnigan [13] for near-neutral stability is presented in dashed line as a benchmark.

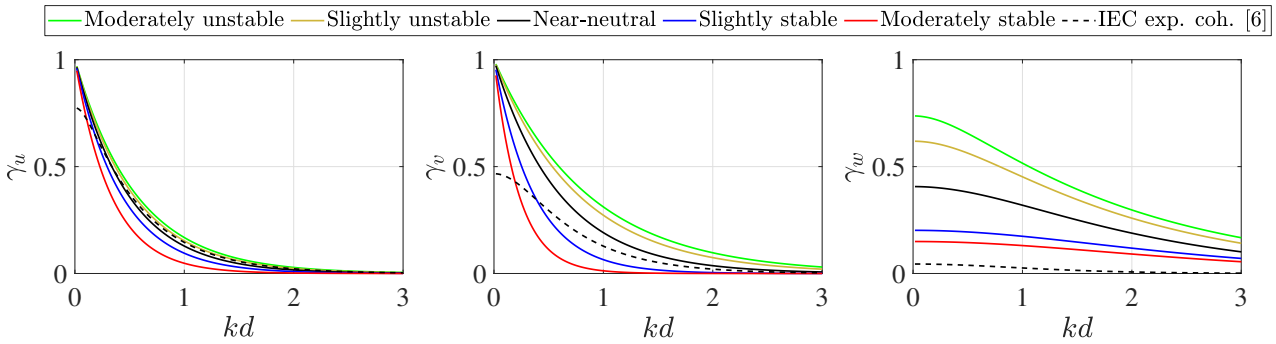

Figure 3. Theoretical co-coherence of the along-wind (left), cross-wind (middle), and vertical (right) velocity components for all considered stability classes for $\overline{u}_{hub} = 12\,\mathrm{m\,s^{-1}}$ and separation distance of $d = 60\,\mathrm{m}$. $k = 2\pi f/\overline{u}_{hub}$ is the wave number. The exponential coherence from IEC 61400-1 [6] for near-neutral stability is presented in the dashed line for comparison.

Table 2. Waves parameters for different mean wind speeds.

	Mean wind speed at hub height [$\mathrm{m\,s^{-1}}$]							
	6	8	10	12	14	16	18	20
H_s [m]	0.5	0.6	0.7	1.1	1.8	2.6	3.5	3.8
T_p [s]	3.5	3.9	3.7	5.2	6.8	8.0	6.5	9.7

2.3. Step 2: Aero-hydro-servo-elastic simulation

SIMA (Simulation Workbench for Marine Application) [21] is used as the aero-hydro-servo-elastic simulation tool. The main environmental loads for the aeroelastic simulations are turbulent wind and waves. The turbulent wind input is as described previously and the wave input is given in Table 2, where reference values were taken from Jacobsen and Godvik [1]. The same wave input is applied for all stability classes for each mean wind speed. Each case is run for 30 min, to match the duration of the wind time series.

The spar wind turbine is modelled following Jonkman [12] for the Phase IV of Offshore

Table 3. Spar wind turbines' key characteristics.

Parameter [unit]	Hywind Scotland	OC3
Rated power [MW]	6	5
Rotor diameter [m]	154	126
Hub height [m above sea level]	98	90
Rated wind speed [$\mathrm{m\,s^{-1}}$]	10	11.4
Water depth [m]	95-120	320
Floater draft [m]	78	120
Mooring [-]	3 lines with crowfoot	3 lines

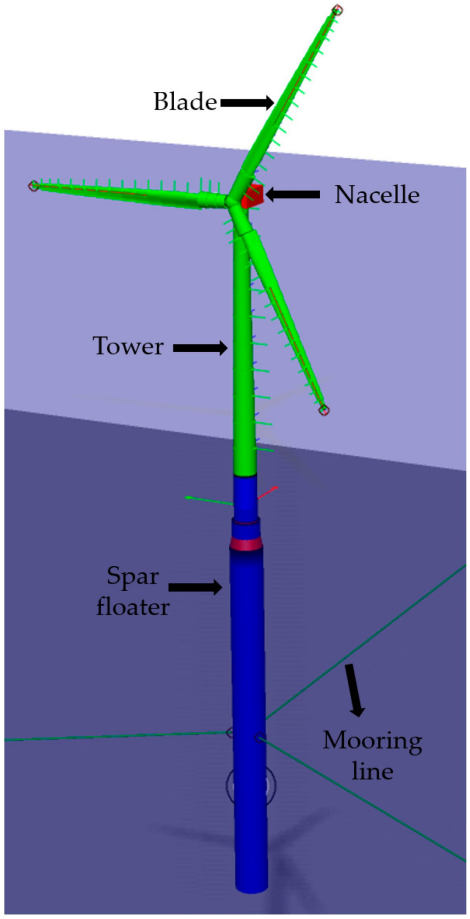

Figure 4. OC3 spar wind turbine modelled in SIMA.

Code Comparison Collaboration (OC3) project, which adopts the NREL's 5 MW turbine. Some important characteristics of the spar WT are provided in Table 3, side-by-side with the Hywind Scotland's spar WT properties as a comparison. Fig. 4 illustrates the OC3 spar WT model in SIMA. The Hywind Scotland WTs have a similar configuration but with a different blade-pitch controller and mooring system, and slightly different dimensions.

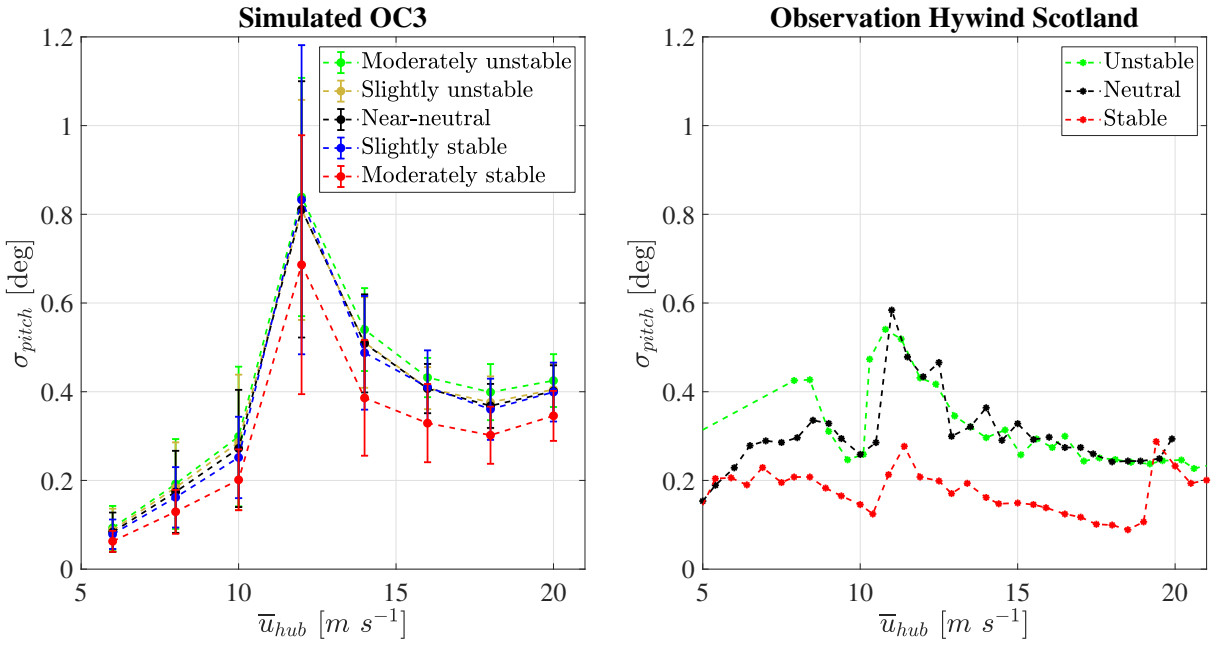

Figure 5. Platform pitch motion: simulation (left) vs observation (right). In the left panel, the circles are the median values from the six seeds, and the error bars indicate the minimum and maximum values from the six seeds.

3. Results and discussion

3.1. Floater motions

We focus herein on the pitch and yaw motions of the floater, which were particularly sensitive to the atmospheric stratification according to the Hywind Scotland observations [1]. The simulated platform pitch and yaw motions are given in the form of standard deviation from a 10 min time series response. Although the simulations were performed for a 30 min duration, only the last 10 min time series were analysed for two main purposes: (1) to avoid the initial transient period and (2) to use a similar averaging time to the one used by Jacobsen and Godvik [1] for Hywind Scotland.

Fig. 5 compares the simulated and the observed platform pitch standard deviations plotted against the mean wind speed for all considered stability classes. In the simulated results, the median values from the six seeds are shown in circles, where the error bars mark the minimum and maximum values from the six seeds at each mean wind speed. The Hywind Scotland observations are presented as the mean values (right panel of Fig. 5) at each mean wind speed bin with an increment of 0.5 m s^{-1}.

Overall, there is a good agreement between the simulations and the observations in Fig. 5. Yet, the magnitude of the platform pitch from the simulations at wind speeds lower than rated are higher than the observations, since there is an advanced blade-pitch controller applied in the Hywind Scotland WTs, while the OC3 model uses only a conventional controller [12]. The advanced blade-pitch controller [22] damps the excessive platform pitch motion of the full-scale spar WTs at Hywind Scotland for wind speeds rated and above. Both the simulated and the observed platform pitch increase with mean wind speed up to the rated wind speed (see Table 3), and then decrease gradually. When using a standard pitch controller for bottom fixed wind turbines for a floating wind turbine, the pitch frequency of the spar floater is nearly similar to the blade pitch frequency of the controller above rated wind speeds. This may account for the differences observed here. Additionally, the use of co-coherence in Eq. 6 may also contribute to

these differences, as the dependency of the decay coefficients on the ratio of vertical separation distance-to-height d_z/z in the MABL [23] is not included. According to Cheynet [23], the use of the Davenport coherence model [20] may lead to overestimation in the simulated wind turbine responses.

Concerning the atmospheric stratification, both the simulations and the observations show that stable conditions yield the lowest platform pitch response of a spar WT, compared to neutral and unstable conditions (Fig. 5). The simulated platform pitch increases from moderately stable to near-neutral and to moderately unstable conditions. Neutral and unstable conditions yield approximately similar magnitudes of platform pitch, both in the simulated and observed responses. Even so, from the simulation, the platform pitch motion under moderately unstable condition is slightly superior to the near-neutral condition for all wind speeds. The observations show that the platform pitch motion under unstable condition is slightly higher than for neutral condition, only at wind speeds lower than the rated.

Similarly, Fig. 6 shows the simulated and the observed platform yaw standard deviations plotted against the mean wind speed for all considered stability classes. In general, there is a similar trend for the platform yaw responses for both the simulations and the observations. The platforms yaw in greater magnitude with wind speed increment, as a higher wind speed induces a higher yaw moment on the rotor. Except for stable stratification, the observation shows mainly higher platform yaw response than the simulation. One of the causes may be due to the larger rotor size of the Hywind Scotland WT than the OC3 model which contributes to a larger yaw moment experienced by the platform. Also, the Hywind Scotland observations considered only periods when the active yaw damping control was disabled [1].

The simulated and the observed platform yaw motions show a similar dependency on the atmospheric stratification as shown in Fig. 6. The simulated platform yaw increases consistently from moderately stable to near-neutral and to moderately unstable conditions. The same is also noted from the Hywind Scotland observation, except that the platform yaw responses under neutral and unstable conditions are roughly of the same magnitude.

3.2. Discussion

Albeit there is a reasonable agreement between the simulated and the observed platform responses, a notable discrepancy in magnitude is especially seen when comparing stable and unstable conditions. The simulations show a systematic change of the platform responses with the atmospheric stability, as it shifts from moderately stable to moderately unstable. This behaviour follows the trend of the target turbulent wind spectra, particularly at dimensionless frequencies below 0.05 shown in Fig. 2. The natural frequencies of large floating wind turbines are typically below 0.2 Hz, which coincide with the observed higher spectral energy of the velocity components in unstable atmospheric conditions. On the other hand, there are larger discrepancies of platform motion responses for stable and unstable conditions from the Hywind Scotland observations. The estimation of atmospheric stability at the Hywind Scotland site was in fact quite crude due to the limited observation available i.e. by measuring the temperature difference between the air and the sea. This method is most likely unable to resolve atmospheric stability with a fine resolution. Even so, the observed full-scale measurements show a clear difference of platform motion responses between unstable and stable conditions that were successfully reproduced in the simulations. There is no rule as to which one is the best method to categorise atmospheric stability. Nonetheless, it is recommended to consider both the temperature and momentum fluxes to determine the degree of atmospheric stratification [13]. As a result, there is an implied uncertainty on how stable is actually 'stable stability class', and how unstable is actually 'unstable stability class' in the Hywind Scotland study.

The influence of co-coherence on the floater yaw response between the simulations and the observations at Hywind Scotland can not be fully resolved, since to the authors' knowledge, there

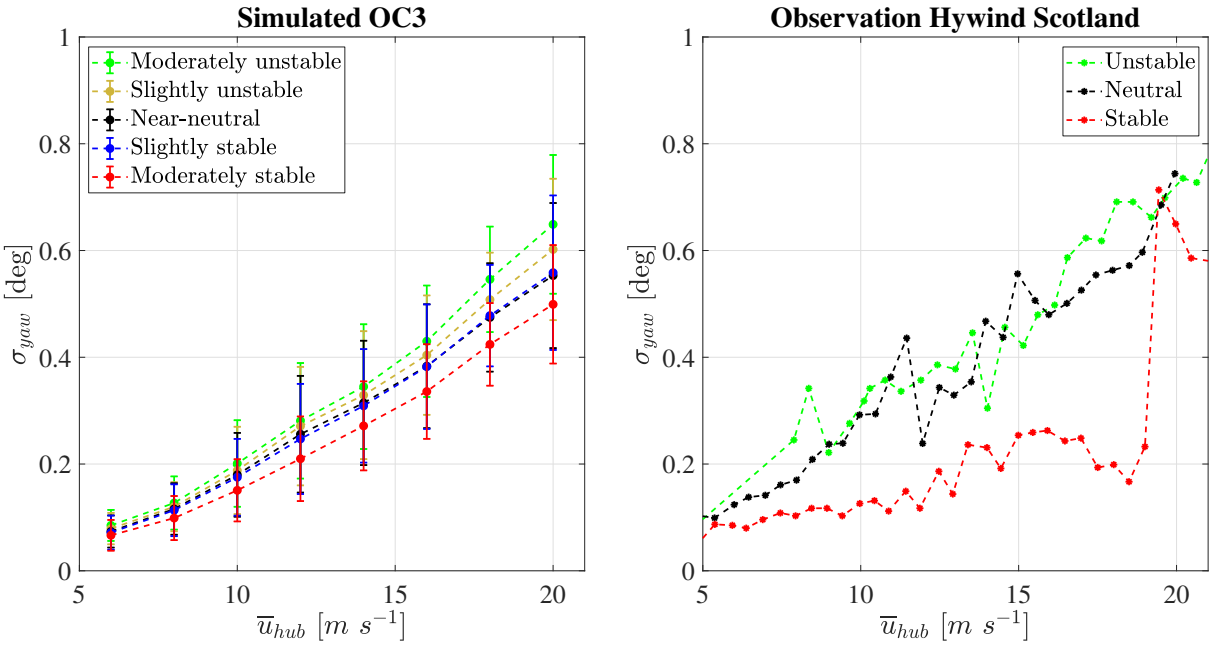

Figure 6. Platform yaw motion: simulation (left) vs observation (right). Simulation: the circles are the median values from the six seeds, and the error bars indicate the minimum and maximum values from the six seeds. Observation: the stars mark the mean values at each mean wind speed bin.

exist only limited studies that focus on the coherence for lateral separations at MABL, e.g. by Kristensen and Jensen [25]. The recent COTUR study [24] has attempted to measure co-coherence for lateral separation at different heights at MABL but has not been classified as a function of atmospheric stability. The floater yaw response of a spar WT has been shown to be susceptible to the spatial variation of turbulent wind, particularly in the lateral direction [26], where a lower magnitude of lateral-separation co-coherence may cause a higher platform yaw response. In the simulation, the target lateral-separation co-coherences are applied similarly to the vertical-separation co-coherences due to the absence of information on the lateral-separation co-coherence from FINO1 measurement. As highlighted by Solari and Piccardo [27] also Saranyasoontorn et al. [28], the behaviour of lateral-separation co-coherence differs from vertical-separation co-coherence for each velocity component. It is unclear whether the assumption of using the same values for lateral-separation and vertical-separation co-coherences is reasonable for floating WT's aeroelastic simulations. Assuming identical co-coherence decays for lateral and vertical separations is likely an oversimplification, which is partly reflected by the discrepancies between the simulated and the measured spar floater responses. Therefore, additional measurements of the co-coherence for lateral separations are needed in the MABL, to properly model the turbulent wind loading on the rotor of state-of-the-art OWTs.

4. Conclusion

This study compared the responses of a simulated spar wind turbine (WT) exposed to synthetic wind fields generated based on real measurements in the marine atmospheric boundary layer (MABL), and the actual observations of spar WT responses at Hywind Scotland Wind Farm. Although the simulated spar WT differs in terms of size, control system, and mooring system from the Hywind Scotland WT, we aim to focus on the comparison of the platform pitch and yaw motions with respect to various atmospheric stratifications. Five stability classes are defined in

the simulations, based on the non-dimensional stability parameter $\zeta = z/L$, while three stability classes are identified from the observation as measured by the temperature difference between the air and sea.

Aeroelastic simulations using the Pointed-Blunt spectral wind model were able to reproduce similar variations and trends in the platform pitch and yaw motion responses of a 5 MW spar WT as a function of atmospheric stability when compared to the full-scale observations of Hywind Scotland spar WT. Both the simulated and the observed responses show that a spar-type WT experiences larger platform pitch and yaw motions in unstable atmospheres. This demonstrates the importance of including atmospheric stratification in the fatigue design of large floating offshore WTs since the occurrence of non-neutral atmospheres is prominent at MABL.

The simulations show a systematic decrease in platform pitch and yaw magnitudes when the atmospheric stability moves from moderately unstable to moderately stable, as also noted from the Hywind Scotland observations. However, some discrepancies were found between the observed and the simulated motion responses for unstable and stable conditions. The different methods used to classify atmospheric stratification at the Hywind Scotland Wind Farm and in the simulations may partly explain this discrepancy. Additionally, the implementation of identical co-coherences for lateral and vertical separations may, to some extent, contribute to the noted discrepancy.

The platform pitch motion increases with the mean wind speed up to the rated speed and then decreases due to the negative damping effect, which was seen both in the simulation results and the observations. The observation suggests a smaller negative damping response than the simulation, because of the implementation of an advanced blade-pitch controller. Also, the simulations adopted a co-coherence model where the decay coefficients are independent on the measurement height or the separation distance, which may result in a larger negative damping effect due to an overestimation of the wind loading. Therefore, aeroelastic simulations of offshore wind turbines (OWTs) require accurate co-coherence modelling to properly estimate the wind loading, as emphasised in the present study.

References

[1] Jacobsen A and Godvik M Influence of wakes and atmospheric stability on the floater responses of the Hywind Scotland wind turbines 2021 *Wind Energy* **24(2)** 149–161
[2] Lee J A, Hacker J P, Delle Monache L, Kosović B, Clifton A, Vandenberghe F, and Rodrigo, J S Improving wind predictions in the marine atmospheric boundary layer through parameter estimation in a single-column model 2017 *Mon. Weather Rev.* **145(1)** 5–24
[3] Sathe A, Mann J, Barlas T, Bierbooms W A A M, and Van Bussel G J W Influence of atmospheric stability on wind turbine loads 2013 *Wind Energy* **16(7)** 1013–1032
[4] Holtslag M C, Bierbooms W A A M, and Van Bussel G J W Wind turbine fatigue loads as a function of atmospheric conditions offshore 2016 *Wind Energy* **19(10)** 1917–1932
[5] Mann J The spatial structure of neutral atmospheric surface-layer turbulence 1994 *J. fluid mech.* **273** 141–168
[6] IEC 61400-1 Wind Turbines Part 1: Design Requirements 2005
[7] Chougule A, Mann J, Kelly M, and Larsen, G C Simplification and validation of a spectral-tensor model for turbulence including atmospheric stability 2018 *Bound. Lay. Met* **167(3)** 371–397
[8] Højstrup J Velocity spectra in the unstable planetary boundary layer 1982 *J. of Atm. Sci.* **39(10)** 2239–2248
[9] Cheynet E, Jakobsen J B, and Reuder J Velocity spectra and coherence estimates in the marine atmospheric boundary layer 2018 *Bound. Lay. Met* **169(3)** 429–460
[10] Putri R M, Obhrai C, and Knight J M Offshore wind turbine loads and motions in unstable atmospheric conditions 2019 *J. Phys.: Conf. Ser.* **1356(1)** 012016
[11] Cheynet E Wind field simulation (the fast version) 2020 `https://zenodo.org/record/3774136`
[12] Jonkman J 2010 *Definition of the Floating System for Phase IV of OC3* (Golden: National Renewable Energy Lab.)
[13] Kaimal J C and Finnigan J J 1994 *Atmospheric boundary layer flows: their structure and measurement* (New York: Oxford University Press)
[14] Watson, B H H 1975 *A study of the statistical approach to wind loading* (Cape Town: University of Cape Town)

[15] Shinozuka M, and Jan, C M Digital simulation of random processes and its applications 1972 *J. sound and vibr.* **25(1)** 111–128
[16] Veers P S 1988 *Three-dimensional wind simulation* (Albuquerque: Sandia National Labs.)
[17] DNV RP-C205 Environmental conditions and environmental loads 2010
[18] Charnock H Wind stress on a water surface 1955 *Quar. J. of the Royal Met. Soc.* **81(350)** 639–640
[19] Wu J Wind-stress coefficients over sea surface near neutral conditions—A revisit 1980 *J. Phys. Oceanogr.* **10(5)** 727–740
[20] Davenport A G The Spectrum of Horizontal Gustiness near the Ground in High Winds 1961 *Q. J. R. Meteorol. Soc.* **87** 194–211
[21] SINTEF Simulation workbench for marine applications Accessed April 2022 `https://www.sintef.no/en/software/sima/`
[22] Skaare B Development of the Hywind Concept 2017 *Int. Conf. Offsh. Mech. and Arctic Eng.* **57779** V009T12A050
[23] Cheynet E Influence of the measurement height on the vertical coherence of natural wind 2019 *In Conf. the Italian Assoc. Wind Eng.* 207–221
[24] Cheynet E et al. The COTUR project: remote sensing of offshore turbulence for wind energy application 2021 *Atm. Measur. Techniq.* **14(9)** 6137–6157
[25] Kristensen, L and Jensen N O Lateral coherence in isotropic turbulence and in the natural wind 1979 *Bound. Lay. Met* **17(3)** 353—373
[26] Godvik M 2016 *Influence of wind coherence on the response of a floating wind turbine* In: Science Meets Industry
[27] Solari G and Piccardo G Probabilistic 3-D turbulence modeling for gust buffeting of structures 2001 *Prob. Eng. Mech.* **16(1)** 73–86
[28] Saranyasoontorn K, Manuel L, and Veers P S A comparison of standard coherence models for inflow turbulence with estimates from field measurements 2004 *J. Sol. Energy Eng.* **126(4)** 1069–1082